Chinese Chemical Letters 32 (2021) 3189–3194

Contents lists available at ScienceDirect

Chinese Chemical Letters

journal homepage: www.elsevier.com/locate/cclet

Communication

Microwave-assisted synthesis of colorimetric and fluorometric dual-functional hybrid carbon nanodots for Fe^{3+} detection and bioimaging

Yupeng Shi[a], Jingjing Liu[a], Yong Zhang[a], Jianfeng Bao[a], Jingliang Cheng[a,*], Changqing Yi[b,*]

[a] Key Laboratory of Functional Magnetic Resonance Imaging and Molecular Imaging (Henan Province), Department of MRI, The First Affiliated Hospital of Zhengzhou University, Zhengzhou 450052, China
[b] Guangdong Provincial Engineering and Technology Center of Advanced and Portable Medical Devices, School of Biomedical Engineering, Sun Yat-sen University, Shenzhen 518107, China

ARTICLE INFO

Article history:
Received 6 December 2020
Received in revised form 6 February 2021
Accepted 8 March 2021
Available online 11 March 2021

Keywords:
Paper-based chip
Carbon nanodots
Colorimetric
Fluorescence
Fe^{3+}ions detection
Dual-functional

ABSTRACT

Carbon nanodots (CDs) based fluorescent nanoprobes have recently drawn much attention in chemo-/bio-sensing and bioimaging. However, it is still challenging to integrate the colorimetric and fluorometric dual readouts into a single CD. Herein, novel hybrid CDs (HCDs) are prepared by a simple microwave-assisted reaction of citric acid (CA), branched polyethyleneimine (BPEI) and potassium thiocyanate (KSCN). As-prepared HCDs show extraordinary properties, including excitation-dependent emission, satisfactory fluorescence quantum yield (46.8%), excellent biocompatibility and optical stability. Significantly, the fluorescence intensity at 450 nm exhibits linear correlation over the Fe^{3+} concentration from 1 μmol/L to 150 μmol/L with a detection limit (LOD) of 52 nmol/L. Meanwhile, the solution color changes from colorless to orange, and the absorbance at 460 nm increased linearly with Fe^{3+} concentration ranging from 0.02 mmol/L to 5 mmol/L (LOD: 3.4 μmol/L). All the evidence illustrates that the HCDs can be conditioned for specific Fe^{3+} sensing with colorimetric and fluorometric dual readouts, which has also been verified with paper-based microchips. The possible mechanism is attributed to the specific interactions between surface functional groups on the HCDs and Fe^{3+}. Additionally, the HCDs are successfully applied in sensing Fe^{3+} in wastewater and living cells, demonstrating its potential applications in future environment monitoring and disease diagnosis.

Iron ions are the most abundant metal ions in our daily lives, and it plays a vital role in various physiological processes such as chain oxygen transport, metabolism and respiration. *etc.* [1,2]. The disorder of Fe^{3+} ions is also related to various diseases such as anemia, diabetes, cancer, Alzheimer's disease, heart failure, which seriously threaten the health of human and quality of life [3,4]. Moreover, excessive iron ion content will also cause a certain degree of pollution to soil and groundwater. Therefore, research interest in developing effective Fe^{3+} monitoring methods is rapidly growing. Although conventional laboratory Fe^{3+} detection methods such as inductively coupled plasma-mass spectrometry (ICP-MS), ICP-atomic emission spectroscopy (ICP-AES), and atomic absorption spectroscopy (AAS) own the high sensitivity and selectivity, the complex procedures and expensive consumption seriously limit their applications outside the laboratory [5,6].

Optical methods are widely recognized as important detection methods for non-destructive analysis [7–9]. In past decades, a series of organic fluorescent probes were designed and achieved satisfactory results for Fe^{3+} quantitation [10,11]. However, toxic reagents were often involved in probe preparation. In addition, most organic fluorescent probes suffer from weak water solubility, which is an obviously disadvantage for the analysis of water samples and living organisms [12].

With the development of nanotechnology, nanomaterials have been extensively designed as optical probes for detecting and/or imaging of Fe^{3+} in aqueous solution and biological cells due to their amazing properties such as simple preparation, easy functionalization, high photo-stability and low toxicity [13–18]. For example, nanoprobes based on gold nanoparticles, metal nanoclusters,

* Corresponding authors.
E-mail addresses: fccchengjl@zzu.edu.cn (J. Cheng), yichq@mail.sysu.edu.cn (C. Yi).

https://doi.org/10.1016/j.cclet.2021.03.022
1001-8417/

fluorescent silica nanoparticles, semiconductor quantum dots, upconverting nanoparticles have been explored for Fe^{3+} sensing using various strategies [19–22]. Very recently, fluorescent carbon nanodots (CDs) have received much attention in various research areas such as energy, electronics, catalysis, inks, and biomedical sensing [23–28]. Especially, their superior optical properties, excellent biocompatibility, green synthesis, and low cost make CDs effective optical sensors to monitor metal ions, small biomolecules, and proteins [29–36]. For example, Song *et al.* presented a bright and color-tunable nitrogen-doped CD by using aminosalicylic acid as a precursor. The enriched phenolic hydroxyl group on the CD surface can easily form complex with Fe^{3+} and thereafter change fluorescence of the CD. This emission property of the CDs is successfully employed for sensing Fe^{3+} in living cells [36]. Nevertheless, most of these ion detection methods rely on a single readout, either fluorometric or colorimetric signals.

The colorimetric and fluorometric dual readouts not only provide high sensitivity of fluorescence detection but also allows direct visual analysis of samples by simple colorimetry without complex detection condition [37,38]. Chan *et al.* developed a new fluorometric immunochromatographic test strip based on the assembly of fluorescent Pdots and gold nanorods nanocomposites. This detection system can fast and accurately detect prostate-specific antigen (PSA) within 10 min by colorimetric and fluorometric dual signals [39]. Our previous work also attempted to develop this type of colorimetric and fluorometric dual-readout sensor. We combined the fluorescence properties of CDs with the color change of AuNPs to achieve bimodal detection of GSH in serum [31]. However, such nanoprobes require a combination of two separate components of colorimetric and fluorometric modules with complex construction processes. Therefore, integration of colorimetric and fluorometric dual-signals into one single system, and development of a dual-functional nanoprobe with simple fabrication, low-cost, ease-to-use and good biocompatibility are extremely attractive.

In this study, N, S-doped fluorescent CDs were synthesized by a simple one-pot microwave-assisted method, and the as-prepared CDs were demonstrated for Fe^{3+} sensing with colorimetric and fluorometric dual readouts (Scheme 1). The reported nanoprobe has several advantages. Firstly, the precursors are cheap, the preparation process is facile, optical stability is good, and the cytotoxicity is negligible. Secondly, Fe^{3+} can be sensitively detected in a wide range of 1.0 μmol/L to 150 μmol/L, and the detection limit is as low as 52 nmol/L. Besides, the obvious color change from colorless to orange along with the increasing Fe^{3+} concentration can be observed by bare eyes. This detection method is not limited to sensing in solution, also can be applied in the differential detection of Fe^{3+} on the paper-based chips. In addition, the as-prepared CDs with excellent biocompatibility were also demonstrated for effectively imaging intracellular Fe^{3+}.

In this study, the HCDs synthesis was accomplished by one-pot microwave reaction with CA, branched PEI and KSCN as the precursors (Scheme 1). The entire synthesis process is very efficient and only takes 3 min. After purification, the morphology of the as-prepared HCDs was examined by transmission electron microscope (TEM). As shown in Fig. 1a, HCDs exhibit uniform spherical structure with a diameter of 5−8 nm and can be homogeneously dispersed in aqueous solution. Dynamic light scattering (DLS) measurements demonstrated that the diameter of the HCDs was ~10 nm (Fig. 1b), which is larger than those observed by TEM because of the presence of a hydration layer. High-resolution TEM (HRTEM) in Fig. 1a (inset image) revealed the crystal structure of the HCDs as evidenced by the well-resolved crystal lattice spacing of 0.34 nm. Consistent with HRTEM results, X-ray diffraction (XRD) measurements further confirmed the crystallinity of the HCDs. XRD pattern (Fig. 1c) showed a broad diffraction peak at around 25.1° (~0.34 nm), suggesting that the HCDs were consist of small crystal nuclei with disordered surface [40,41].

FT-IR was performed to characterize the surface functional groups of the HCDs. As shown in Fig. 1d, the broad absorption peak around 3000−3500 cm^{-1} clearly confirmed the existence of O—H and N—H bonds. Meanwhile, the peak at 2768 cm^{-1} was also attributed to vibrations of N—H, indicating the presence of $—NH_2$ on the surface of HCDs. In addition, the existence of C=O bond is evidenced by two peaks located at 1713 and 1399 cm^{-1}, respectively. The stretching vibration of the C—C and/or C—N bonds should be responsible for the absorption peak at 1184 cm^{-1}. In addition, it has characteristic thiocyanate vibrations, including ν_S (C≡N) at 2057 cm^{-1}. All the above evidence indicated that sulfur and nitrogen have been successfully co-doped into the HCDs, and the HCDs contains a variety of surface functional groups (including thiocyanate, hydroxyl, carboxyl and amino).

The optical properties of the HCDs were investigated by UV–vis absorption and photoluminescence (PL) spectra. Fig. S1a (Supporting information) shows the typical absorption spectra of the HCDs. The absorption peak at ~274 nm belongs to π-π^* of C=C bands, while the peak at 342 nm represents the n-π^* of C=O bands, suggesting the existence of carbon core and plenty of carboxyl group on the surface of HCDs [42]. The PL emission spectra were investigated under a series of excitation wavelengths. Fig. S1b (Supporting information) illustrates that the PL emissions of the HCDs are highly dependent on the excitation energy, which is a classical emission property of CDs [38]. Specifically, when the excitation wavelength increases from 300 nm to 540 nm, the emission spectrum of the HCDs correspondingly red-shifted from 420 nm to 600 nm. Meanwhile, the HCDs exhibited the strongest PL emission at ~440 nm under excitation at 360 nm. The HCDs also exhibited a high quantum yield (QY) of 46.8% which was measured in the aqueous solution with quinine sulfate as standard.

Interestingly, not only the fluorescence of the HCDs was effectively quenched by Fe^{3+} ions, but also the color of the HCD solution changed from colorless to orange. The solution of the HCDs is colorless under daylight (inset 2 of Fig. S1a), while it shows

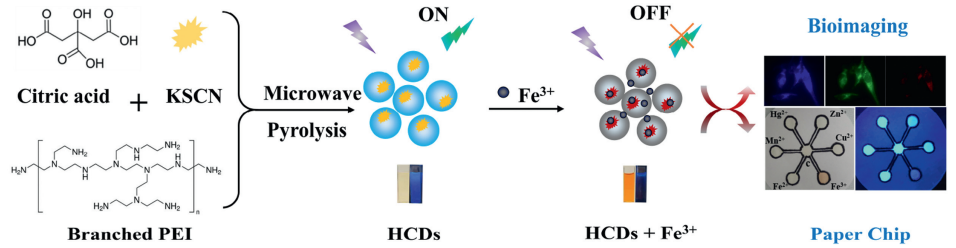

Scheme 1. Schematic representation of the procedure for the synthesis of the HCDs and their application in Fe^{3+} sensing and imaging.

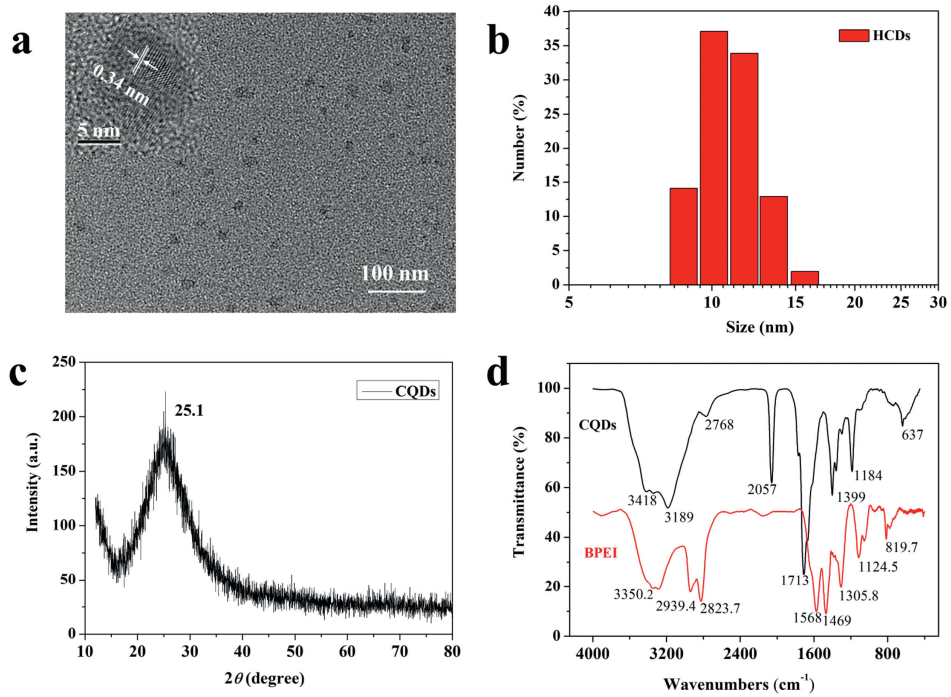

Fig. 1. (a) TEM image and HRTEM image of the HCDs. (b) The corresponding size distribution of the HCDs. (c) XRD spectrum of the HCDs. (d) FT-IR spectrum of the HCDs and branched polyethyleneimine (BPEI).

bright blue emission under 360 nm excitation (inset 5 of Fig. S1b). After adding a colorless and non-fluorescent Fe^{3+} ion solution (inset 1 of Fig. S1a and inset 4 of Fig. S1b), the mixture solution exhibited an orange color (inset 3 of Fig. S1a), and produced fluorescence quench under an ultraviolet lamp (inset 6 of Fig. S1b). It has been well-established that the surface properties of nanoparticles play an important role in their optical behaviors. Possibly due to chelation between the surface functional groups and Fe^{3+}, the surface properties of the HCDs were greatly affected, resulting in both the fluorescence quench of the HCDs *via* electron or energy transfer and color change of the HCD solution [43,44]. More importantly, these changes in the HCD optical properties illustrated their feasibility for Fe^{3+} sensing with both colorimetric and fluorometric signals.

The formation of non-luminescent orange complexes with the absorption spectra around 460 nm between Fe^{3+} and the functional groups of HCDs may be a possible mechanism for this phenomenon. It can be seen from Fig. S2 (Supporting information) that as the temperature increases, the quenching rate coefficient K_{sv} decreases significantly from 0.0303 to 0.0272. However, this quenching effect is not so obvious at low Fe^{3+} concentrations due to the formation of fewer non-luminescent complexes. As the Fe^{3+} concentration increases, this trend becomes more obvious. Therefore, the fluorescence quenching of HCDs by Fe^{3+} might be a static quenching process, which also correlates well with the absorption spectra.

Optical stability is an important indicator for evaluating the physical and chemical properties of the HCDs. As shown in Fig. S3a (Supporting information), the HCDs exhibited a slight pH-dependent behavior in the pH range of 5–11, which was mainly due to protonation/ deprotonation (—NH_2, —OH, —COOH) or hydrolysis (O=C—NH). Similarly, it could be found that as the concentration of KCl increased to 2.0 mol/L, the fluorescent intensity of the HCDs was almost unaffected (Fig. S3b in Supporting infoamation). And Figs. S3c and S3d (Supporting information) revealed that the fluorescent intensity of the HCDs only decreased by ~5.0% even after 100 min of continuous UV irradiation and storage for 6 months. Overall, the above results confirm that the as-prepared HCDs have excellent optical stability, providing a guarantee for its further sensing applications.

The feasibility of the HCDs as colorimetric and fluorometric dual-modal nanoprobe for Fe^{3+} sensing was then evaluated. Fig. 2a showed that after Fe^{3+} ions were added, the HCD solution showed an obvious absorption peak at 460 nm, and as the concentration of Fe^{3+} increases, the absorption intensity at 460 nm gradually

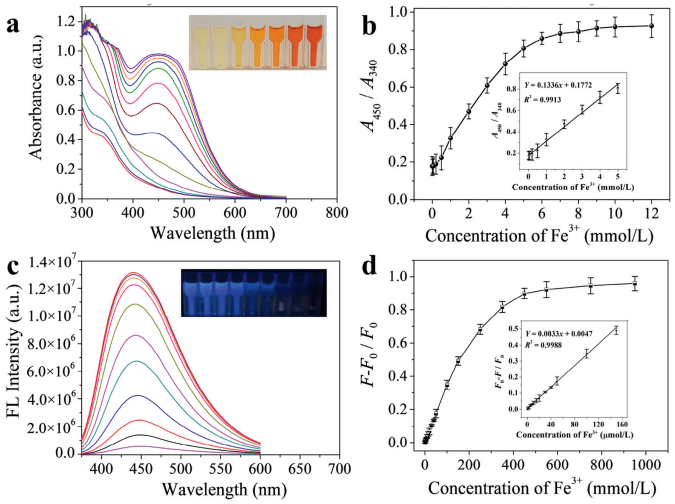

Fig. 2. (a) UV–vis spectra of the HCDs with different concentrations of Fe^{3+} and the relevant inset images. (b) The variation of the absorbance of the HCDs suspension with Fe^{3+} concentration range from 0.02 μmol/L to 12 mmol/L, and the relevant calibration curve. (c) Fluorescence spectra of the HCDs with different Fe^{3+} concentrations and relevant fluorescence photographs under 365 nm excitation. (d) The fluorescent variation of the HCDs by adding different concentrations of Fe^{3+} from 0.2 μmol/L to 950 μmol/L, and the relevant calibration curve.

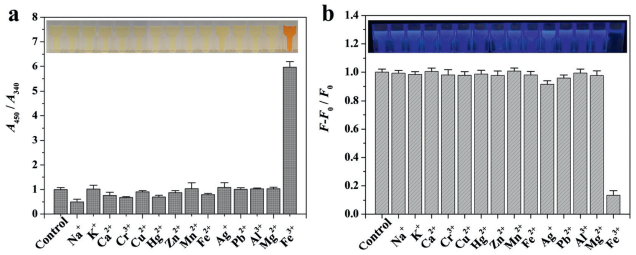

Fig. 3. (a) Absorption ratio A_{450}/A_{340} of the HCDs suspension with various interferent ions (100 μmol/L), and the related photographic images. (b) Fluorescence response of the HCDs in the presence of different metal ions (100 μmol/L), and the related photographic images under UV lamp. F_0 represents the fluorescent intensity of the HCDs in the absence of interferent ions, and F is the fluorescent intensity of the HCDs in the presence of interferent ions.

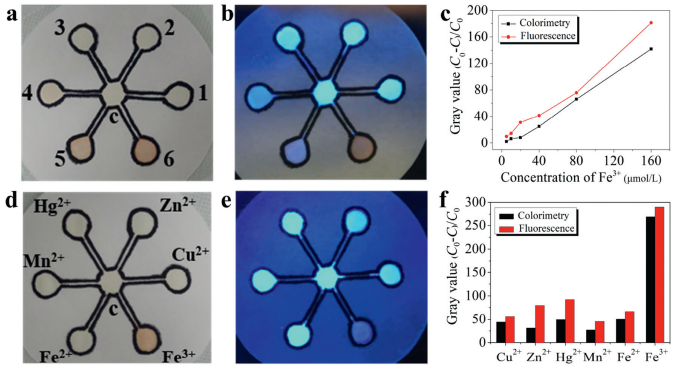

Fig. 4. (a, b) Colorimetric and fluorometric detection of Fe^{3+} ions using filter paper-based chips (The concentrations of Fe^{3+} are 5, 10, 20, 40, 80, 160 μmol/L, respectively). (d, e) Colorimetric and fluorometric differentiation of Fe^{3+} ions from interferent metal ions using filter paper-based chips. (c, f) The corresponding semi-quantitative date analysis of colorimetric and fluorometric signals from filter paper-based chips.

increases. This is consistent with the gradual color change of the HCD solution from colorless to orange as shown in the inset of Fig. 2a. Through quantitative analysis, it was found that the Fe^{3+} concentration in the range of 0.02∼5.0 mmol/L was well correlated with the absorbance of the HCDs at 460 nm with a satisfactory linear relationship ($y = 0.1336x - 0.1772$, $R^2 = 0.9913$) (Fig. 2b). The detection limit (LOD) of the colorimetric method was calculated to be as low as 3.4 μmol/L (LOD = 3σ/S). Meanwhile, along with the increase of Fe^{3+} concentration from 0.2 μmol/L to 950 μmol/L, the fluorescent intensity of the HCDs gradually decreased, and the highest quenching efficiency reached to 94% (Fig. 2c). The Fe^{3+} concentration in the range of 1∼150 μmol/L had a good correlation with the fluorescence quenching efficiency, and the lowest detection limit reached 52 nmol/L (Fig. 2d). Through careful analysis of absorption and emission spectra of the HCD solution in the absence and presence of Fe^{3+}, it was found that after Fe^{3+} was added, the absorbance at ∼460 nm increased while the fluorescence at ∼450 nm gradually decreased (Fig. S1).

To evaluate the specificity of the colorimetric/fluorometric dual signals of the HCDs for Fe^{3+} detection, a concentration of 100 μmol/L potential interfering substances (Ag^+, K^+, Na^+, Ba^{2+}, Ca^{2+}, Fe^{2+}, Mg^{2+}, Mn^{2+}, Ni^{2+} and Zn^{2+}) were prepared. Fig. 3 showed that in the absence of Fe^{3+}, the addition of interfering substances did not cause a substantial change in either the colorimetric or fluorometric signal. In contrast, after the addition of Fe^{3+}, color of the HCDs solution changed obviously (from colorless to orange), and its fluorescence was also substantially quenched. These results validated the high specificity of the HCDs towards Fe^{3+} sensing with both the colorimetric and fluorometric readouts.

The conventional strategies for determining free Fe^{3+} are limited by laborious, time-consuming and expensive laboratory instruments that are difficult to be implemented at the point of care settings. Inspired by the results in solution, the detection of Fe^{3+} using the HCDs was also performed on paper-based chips. Fig. 4a illustrated that as increasing concentration of Fe^{3+} solutions were dropped onto the detection areas, the color of the sensing area enhanced and gradually changed to orange compared with control (only HCDs in the center). Meanwhile, similar fluorescence quench phenomenon was also observed in the paper-based chips (Fig. 4b). When these pictures were converted into gray values using Image J software, the obvious linear change trend of the relevant signals with the increase of Fe^{3+} concentration can be observed, which was of great significance for rapid quantitative analysis (Fig. 4c). The specificity of the paper-based chips was also evaluated. As shown in the Fig. 4, when various interfering metal ion were added onto the detection area of the paper-based chips, it clearly showed that the color and fluorescence intensity in the presence of interfering metal ions barely changed (Figs. 4d–f), suggesting the high specificity of the HCDs towards Fe^{3+} even after being coated onto paper. All these results indicated that the HCDs can be coated onto paper substrate for the potential environmental or biomedical applications.

The potential applications of the HCDs for sensing Fe^{3+} in real sample was also explored. In this study, the quantitative analysis of Fe^{3+} in actual samples was performed by the standard addition method. All water samples were collected from the Jinshui River in Zhengzhou city. Three standard solutions containing different concentrations of Fe^{3+} were added into the water sample, and the Fe^{3+} concentration was determined by colorimetric and fluorometric dual signals. As shown in Table 1, although various interfering metal ions may exist in wastewater, the results showed a good agreement between the added value and the found value. In addition, the quantitative results using the HCDs were also in good agreement with those determined by ICP-AES. The recovery rate was between 95.8%∼112%, showing a promising strategy for rapid and effective detection of Fe^{3+} in real samples. All these results validated that the HCDs can realize Fe^{3+} determination with high accuracy.

MTT assay results confirmed the good biocompatibility of the HCDs. As revealed in Fig. S4 (Supporting information), the cell viability still reached 94%, even after the NHDF cells were incubated with 0.6 mg/mL of the HCDs for 24 h. The low cytotoxicity and good biocompatibility lay the foundation for applying fluorescent HCDs in biomedical imaging. Therefore, the feasibility of HCDs as fluorescent nanoprobes for real-time imaging Fe^{3+} in living cells was examined. After being incubated with 0.2 mg/mL HCDs for 4 h, NHDF cells remained intact (Figs. 5a and e), also indicating the good biocompatibility of the HCDs. After being excited with 405 nm, 458 nm and 514 nm, different imaging channels displayed bright blue (Fig. 5b), green (Fig. 5c) and red (Fig. 5d) fluorescence. This is consistent with the typical CD characteristic of excitation-dependent emission. The HCDs were mainly distributed in the cytoplasm, which is consistent with previous reports that CDs can be mainly enriched in the cytoplasm and cell membrane through endocytosis, but they are difficult to enter the nucleus [45,46].

To study the responsiveness of the HCDs to Fe^{3+} in living cells, 100 μmol/L exogenous Fe^{3+} was added to the HCD pretreated NHDF cells. It could be observed from Figs. 5f–h that after 30 min. incubation, as expected, the fluorescence of the HCDs was effectively quenched. These results validate that the HCDs can

Table 1
The spiked wastewater sample detection of Fe^{3+} by the colorimetric and fluorometric method (mean ± SD, $n = 5$).

Method	Sample	Added (μmol/L)	Measured (μmol/L)	Recovery (%)	RSD (%)	ICP-AES (μmol/L)
Colorimetric method	1	50	47.9 ± 10	95.8	8.4	52.4 ± 2.7
	2	100	106.8 ± 13	106.8	13.7	98.3 ± 5.3
	3	200	192.4 ± 16	96.2	17.0	203.4 ± 8.2
Fluorometric method	4	5	5.2 ± 1.3	104	0.7	4.8 ± 0.8
	5	10	11.2 ± 1.2	112	0.9	10.4 ± 1.3
	6	20	19.4 ± 2.4	97	1.4	20.3 ± 1.3

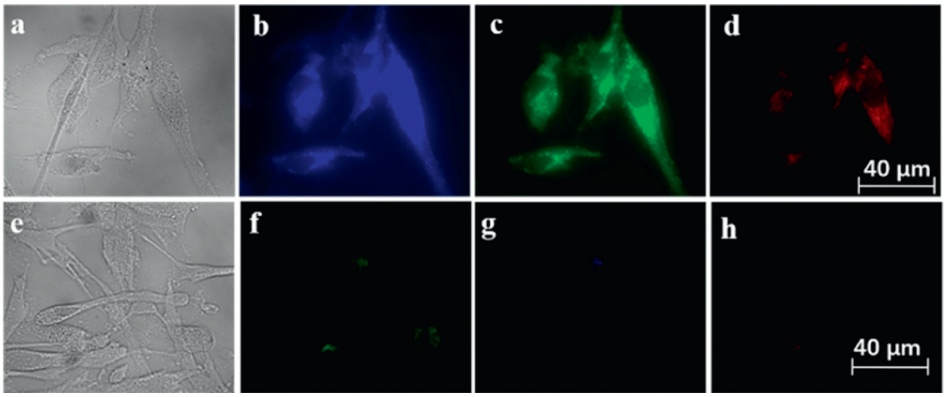

Fig. 5. The fluorescence microscopy images of NHDF cells treated with 0.2 mg/mL HCDs for 4 h, (a-d) in the absence of Fe^{3+} and (e-h) in the presence of Fe^{3+} (100 μmol/L). Images were taken under (a, e) bright-field, (b, f) 405 nm excitation, (c, g) 458 nm excitation, and (d, h) 514 nm excitation. Scale bar =40 μm.

be used as an eff ;ective imaging probe for real-time monitoring intracellular Fe^{3+}.

In this study, the HCDs were successfully prepared by a simple one-step microwave-assisted reaction, and have been successfully conditioned for rapid and sensitive determination of Fe^{3+} with both colorimetric and fluorometric signals *via* either solutions or paper-based chips. This provides an alternative pathway for future development of point-of-care detection. More significantly, the HCDs exhibit good biocompatibility, and have been successfully demonstrated in real-time imaging intracellular Fe^{3+}. There is no doubt that the HCDs draw significance for future applications in environment monitoring and disease diagnosis.

Declaration of competing interest

The authors declare that they have no known competing financial interests or personal relationships that could have appeared to influence the work reported in this paper.

Acknowledgments

Financial support for this work came from the Project of Henan Provincial Medical Science and Technology Research Plan (No. SBGJ202002086), Guangdong Provincial Key Laboratory of Sensing Technology and Biomedical Instruments (No. 2020B1212060077), and Natural Science Foundation of China (Nos. 81901808, 81701752, 81601470).

Appendix A. Supplementary data

Supplementary material related to this article can be found, in the online version, at doi:https://doi.org/10.1016/j.cclet.2021.03.022.

References

[1] N.C. Andrews, Rev. Clin. Exp. Hematol. 4 (2001) 283–301.
[2] F. Thévenod, Met. Ions Life Sci. 18 (2018) 437–467.
[3] S. Dev, J.L. Babitt, Hemodial. Int. 21 (2017) S6–S20.
[4] M. Muñoz, J.A. García-Erce, Á.F. Remacha, J. Clin. Pathol. 64 (2011) 287–296.
[5] W.J. Goldberg, N. Allen, Clin. Chem. 27 (2019) 562–564.
[6] C.S. Muñiz, J.M.M. Gayón, J.I.G. Alonso, A. Sanz-Medel, J. Anal. At. Spectrom. 14 (1999) 1505–1510.
[7] S.J. Zhu, R. Tian, A.L. Antaris, X.Y. Chen, H.J. Dai, Adv. Mater. 31 (2019)1900321.
[8] R.J. Gui, H. Jin, X.N. Bu, et al., Coord. Chem. Rev. 383 (2019) 82–103.
[9] A.L. Vahrmeijer, M. Hutteman, J.R. van der Vorst, C.J.H. van de Velde, J.V. Frangioni, Nat. Rev. Clin. Oncol. 10 (2013) 507–518.
[10] E.M.S. Stennett, M.A. Ciuba, M. Levitus, Chem. Soc. Rev. 43 (2014) 1057–1075.
[11] R.K. Dubey, G. Knorr, N. Westerveld, W.F. Jager, Org. Biomol. Chem. 14 (2016) 1564–1568.
[12] T.X. Tang, W.B. Guo, Y.P. Zhang, D.M. Xu, J. Fluoresc. 29 (2019) 445–450.
[13] J.J. Zhang, F.F. Cheng, J.J. Li, J.J. Zhu, Y. Lu, Nano Today 11 (2016) 309–329.
[14] C.X. Wang, Y.J. Huang, K.L. Jiang, M.G. Humphrey, C. Zhang, Analyst 141 (2016) 4488–4494.
[15] Y.P. Shi, H. Zhang, Z.F. Yue, Z.M. Zhang, K.S. Teng, M.J. Li, C.Q. Yi, M.S. Yang, Nanotechnology 24 (2013) 375501.
[16] J. Shangguan, J. Huang, D. He, et al., Anal. Chem. 89 (2017) 7477–7484.
[17] B. Shi, Y. Su, L. Zhang, et al., ACS Appl. Mater. Interfaces 8 (2016) 10717–10725.
[18] S. Yang, C. Zhu, J. Song, L. He, Y. Lin, ACS Appl. Mater. Interfaces 9 (2017) 7399–7405.
[19] W. Yang, C.G. Zhang, H.Y. Qu, H.H. Yang, J.G. Xu, Anal. Chim. Acta 503 (2004) 163–169.
[20] J. Ma, Y.H. Chen, Z. Hou, W. Jiang, L. Wang, Biosens. Bioelectron. 43 (2012) 84–87.
[21] S. Ghosh, U. Anand, S. Mukherjee, Anal. Chem. 86 (2014) 3188–3194.
[22] M. Kumar, P. Zhang, Biosens. Bioelectron. 25 (2010) 2431–2435.
[23] J.K. Zhao, X. Chen, K.H. Ho, et al., Chin. Chem. Lett. 32 (2021) 66–86.
[24] Z.H. Kang, Y. Liu, J. Gao, M.M. Zhu, Inorg. Chem. Front. 4 (2017) 1963–1986.
[25] E.B. Secor, M.C. Hersam, J. Phys. Chem. Lett. 6 (2015) 620–626.
[26] S.J. Zhu, Q.N. Meng, L. Wang, et al., Angew. Chem. Int. Ed. 125 (2013) 4045–4049.
[27] Y.N. Fang, J. Jia, J. Yang, J.H. Zheng, C.Q. Yi, Chin. Chem. Lett. 29 (2018) 1277–1280.
[28] M. Xiao, Z.G. Liu, N.X. Xu, et al., ACS Sen. 5 (2020) 870–878.
[29] S.Y. Lim, W. Shen, Z.Q. Gao, Chem. Soc. Rev. 44 (2015) 362–381.
[30] Y.Q. Dong, R.X. Wang, G.L. Li, et al., Anal. Chem. 84 (2012) 6220–6224.
[31] Y.P. Shi, Y. Pan, H. Zhang, et al., Biosens. Bioelectron. 56 (2014) 39–45.
[32] M.D. Xu, Z.Q. Gao, Q. Zhou, et al., Biosens. Bioelectron. 86 (2016) 978–984.
[33] Z.M. Zhang, Y. Pan, Y.N. Fang, et al., Nanoscale 8 (2015) 500–507.

[34] Y.M. Xu, L.H. Yan, M.M. Yue, Y. Yu, Nano 14 (2019) 1950014.
[35] Y. Song, C.Z. Zhu, J.H. Song, H. Li, H.Y. Lin, ACS Appl. Mater. Interfaces 9 (2017) 7399–7405.
[36] Y.L. Zhang, S.J. Qi, Z.G. Liu, et al., Mat. Sci. Eng. C: Mater. 61 (2016) 207–213.
[37] J. Huang, J.F. Shangguan, Q.P. Guo, et al., Analyst 144 (2019) 4917–4924.
[38] Y.N. Fang, L.F. Zhou, J. Zhao, Y. Zhang, C.Q. Yi, Carbon 166 (2020) 265–272.
[39] P.Y. You, F.C. Li, M.H. Liu, Y.H. Chan, ACS Appl. Mater. Interfaces 11 (2019) 9841–9849.
[40] Y.N. Fang, L.F. Zhou, J. Yang, J.K. Zhao, C.Q. Yi, ACS Appl. Bio Mater. 3 (2020) 3761–3769.
[41] Z. Tang, K. Jiang, S. Sun, S. Qian, Y. Wang, H. Lin, Analyst 144 (2019) 468–473.
[42] H. Ding, S. Yu, J. Wei, H. Xiong, ACS Nano 10 (2016) 484–491.
[43] S. Liu, N. Zhao, Z. Cheng, H. Liu, Nanoscale 7 (2015) 6836–6842.
[44] J. Zhu, S. Sun, K. Jiang, Y. Wang, W. Liu, Biosens. Bioelectron. 97 (2017) 150–156.
[45] Y.P. Shi, Y. Pan, J. Zhong, et al., Carbon 93 (2015) 742–750.
[46] Y. Pan, J. Yang, Y.N. Fang, et al., J. Mater. Chem. B 5 (2017) 92–101.